JOURNAL OF COMPUTATIONAL PHYSICS 16, 342–359 (1974)

Shaping the Force Law in Two-Dimensional Particle-Mesh Models

J. W. EASTWOOD AND R. W. HOCKNEY

Computer Science Department, Reading University, Reading, RG6 2AX, Berkshire, England

Received November 28, 1973; revised August 4, 1974

A general two-dimensional theory is presented for the choice of charge-sharing schemes in particle-mesh algorithms. An ordered hierarchy of schemes is obtained in which the lowest orders are represented by the familiar nearest-grid-point (NGP) and cloud-in-cell (CIC) schemes. Of the higher order nine-point charge-sharing schemes the triangular-shaped and gaussian-shaped cloud are favored. The theory is also given for the shaping of the short-range force law by the introduction of potential-correction coefficients which modify the multiplying factor used in the calculation of the potential by Fourier transform methods. Empirical results are given demonstrating the correctness of the theory and showing that the angular anisotropy of the force law can be reduced from 50% for NGP or CIC to less than the 0.5 % by the above methods.

1. INTRODUCTION

The economy of representing the dynamical central force interaction of an ensemble of particles on a mesh rather than evaluating the sum of interparticle forces at each time step, is now well established [1]. In this paper, we shall be concerned only with the quasistatic type of particle-mesh calculation, where potentials are only implicit functions of time. The earliest and simplest of the particle-mesh schemes devised is the nearest-grid-point (NGP) scheme [2]. The total charge of each particle is assigned to the center of the cell in which it lies for the purpose of evaluating charge sums and forces. In consequence, the particle has an effective size equal to that of the cell, and experiences no self-force. However, the speed of the algorithm is, in many applications, outweighed by poor energy conservation [3] and nonphysical grid interactions [4–7] resulting from the coarseness of the force representation.

Several variations on the theme set by NGP have appeared in the literature; Morse and Nielsen, in their particle-in-cell scheme [8, 9], used bilinear interpolation on the electric field for particle pushing, together with inverse interpolation (area weighting) on charge assignments. Birdsall *et al.* [10] devised an equivalent scheme, the cloud-in-cell (CIC) method, where the interpolating function is "carried" with the particle, leading to the useful concept of the finite-sized

particle. A compromise between the speed of NGP and the improved precision of CIC has been used by Orens *et al.* [11], where the charge assignment is quantized by using a subcell containing a mesh of precalculated weights. Kruer *et al.* [12, 13] have introduced the use of multipole expansions about grid points, giving an interesting and powerful method of devising improvements to NGP. Lewis [14, 15] has developed an elegant Lagrangian formulation for generating schemes which have energy constants in the limit $\Delta t \to 0$; unfortunately, his schemes do not in practice show the clear-cut advantages that the theory suggested [16].

A new approach to the particle-mesh calculations is introduced in Part I of this paper. The concept of the finite-sized particle [2] and a splitting of the problem into a "short-range" and a "long-range" part are central to the viewpoint adopted. The regular mesh is treated as an array of expansion centers rather than as a finite-difference mesh, and the finite-difference approximation to the point differential (Poisson's) potential relationship is replaced by an action-at-a-distance expression for the potential.

In Sections 2 and 3, we shall see that the error in the force between particles of large separation is reduced by suitably choosing the charge-sharing scheme. Section 4 is concerned with the short-range force. There, it is show how the Green's function in the potential-solver may be adjusted to offset the anisotropy resulting from charge sharing and potential differencing.

Empirical results are given in Part II which demonstrate the effectiveness of the methods described in Part I. Section 5 covers the choice of charge-sharing scheme and potential-solver, in order to obtain the best long-range force. The effect of cloud shape on the short-range force is given in Section 6. Section 7 gives the results obtained with the introduction of both two and eight potential-correction coefficients. Overall it is demonstrated that the angular anisotropy of the mesh force can be reduced from 50% for NGP and CIC to 0.5% for the best scheme given here, the Quiet Particle Mesh (QPM) model.

Part I. General Two-Dimensional Theory

2. Charge-Sharing Constraints

Assuming coulombic forces, the field may be expressed as a function of the complex variable z, where z is the position of the field point. In particular, the field due to a cylindrical rod of charge q per unit length and of radius a located at $z = 0$ is

$$E_c(z) = E_x - iE_y \tag{1}$$

$$= q/2\pi\epsilon_0 z; \qquad |z| > a. \tag{2}$$

The consequence of representing such a charged rod by charges assigned to a square mesh with spacing unity is to change the (complex) electric field to

$$E_{s,t} = \frac{q}{2\pi\epsilon_0} \sum_{s',t'} \frac{w_{s',t'}(z_0)}{z_{s,t} - z_{s',t'}}, \tag{3}$$

where $z_{s,t} = s + it$ is the position of mesh point (s, t), $w_{s',t'}(z_0)$ is the fraction of the charge assigned to mesh point (s', t') from the source charge at z_0, and $E_{s,t}$ is the approximate field at mesh point (s, t). The sum on the right-hand side of (3) is taken over all mesh points.

Introducing the ratio, $\epsilon_{s',t'}$, of the distance of mesh point (s', t') from the source point to the distance of the field from source point

$$\epsilon_{s',t'} = (z_{s',t'} - z_0)/(z_{s,t} - z_0) \tag{4}$$

enables (3) to be written

$$E_{s,t} = E_c \sum_{s',t'} w_{s',t'}(z_0) \sum_{n=0}^{\infty} \epsilon_{s',t'}^n \tag{5}$$

for $| \epsilon_{s',t'} | < 1$.

We obtain from (5) the orthogonal expansion of the fractional error in the field:

$$\xi = (E_{s,t} - E_c)/E_c \tag{6}$$

$$= \sum_{n=1}^{\infty} \xi_n e^{-in\theta} \tag{7}$$

where

$$\theta = \arg(z_0 - z_{s,t}). \tag{8}$$

Since ξ_n decays like $| z_0 - z_{s,t} |^{-n}$, an ordered set of independent charge-assignment constraints may be constructed by setting $\xi_n = 0$; $n = 0, 1, 2, \ldots$. For instance, an Mth-order scheme has

$$\xi = \sum_{n=M+1}^{\infty} \xi_n e^{-in\theta}, \tag{9}$$

and charge weights chosen such that

$$\xi_n = \frac{1}{| z_0 - z_{s,t} |^n} \sum_{s',t'} w_{s',t'}(z_0)(z_0 - z_{s',t'})^n \tag{10}$$

$$= 0, \qquad \text{all} \quad n \in [0, M]. \tag{11}$$

The constraint equation of order n, given by setting (10) to zero, is

$$\sum_{s',t'} w_{s',t'}(z_0)\, z_{s',t'}^{n} = z_0{}^{n}. \tag{12}$$

The same ordering of the error as given by (9), and the same constraints as given by (12) arise when the long-range potential, potential energy or interparticle force are treated in a similar manner. In the calculation of the interparticle force and interparticle potential energy, the interpolation function is assumed to be identical to the charge weighting function in order that momentum is exactly conserved.

The assumption that the field is analytic must be dropped for noncoulombic forces. For such forces, we denote the "true" field $\mathbf{E}_c$ and mesh-calculated approximate field, $\mathbf{E}_{s',t'}$, by vectors lying in the (x, y) plane:

$$\begin{aligned} \mathbf{E}_c &= \mathbf{E}_c(x, y), \\ \mathbf{E}_{s,t} &= \sum_{s',t'} w_{s',t'}(x_0, y_0)\, \mathbf{g}(s - s', t - t'). \end{aligned} \tag{13}$$

$w_{s',t'}(x_0, y_0)$ is the charge assigned to mesh point (s', t') from a charge at (x_0, y_0) and $\mathbf{g}$ is the Green's function appropriate to the particular force law. Expand (13) about the source to field point vector $\mathbf{x}$.

$$\mathbf{x} = (s - x_0, t - y_0) \tag{14}$$

gives

$$\mathbf{E}_{s,t} = \sum_{s',t'} w_{s',t'}(x_0, y_0) \sum_{n,m=0}^{\infty} \frac{\Delta x^m \Delta y^n}{m!\, n!} \frac{\partial^{m+n}}{\partial x^m\, \partial y^n} \mathbf{g}\Big|_{\mathbf{x}}, \tag{15}$$

where

$$\begin{aligned} \Delta x &= x_0 - s', \\ \Delta y &= y_0 - t'. \end{aligned} \tag{16}$$

The zero $(m + n = 0)$ and first-order $(m + n = 1)$ constraints given by (15) coincide with those for the coulombic force. Higher-order constraints are more severe. For instance, to get (15) to agree with $\mathbf{E}_c$ to second order ($m + n = 3$ for the leading remainder term) we require that the second-order constraint

$$\sum_{s',t'} w_{s',t'} \mid z_{s',t'} \mid^2 = \mid z_0 \mid^2 + 2C \tag{17}$$

be satisfied in addition to those given by $n = 0, 1$ in (2) and that $\mathbf{g}$ be chosen to satisfy

$$\mathbf{g} + (C/2)\, \nabla^2 \mathbf{g} = \mathbf{E}_c + O(\Delta^3), \tag{18}$$

where C is some constant. Setting $C = \frac{1}{4}$ and interpreting the Laplacian in (19) as the nine-point finite-difference approximation

$$\nabla^2\phi_{s,t} = \tfrac{1}{8}[6S_1 + S_2 - 28]\,\phi_{s,t}\,, \tag{19}$$

where the symmetric sums S_1 and S_2 are defined as

$$S_1(\phi_{s,t}) = \phi_{s,t+1} + \phi_{s,t-1} + \phi_{s+1,t} + \phi_{s-1,t}\,, \tag{20}$$

$$S_2(\phi_{s,t}) = \phi_{s+1,t+1} + \phi_{s+1,t-1} + \phi_{s-1,t+1} + \phi_{s-1,t-1} \tag{21}$$

gives the spline fitting equations through to second order. Note that with spline fitting schemes, the charge weights are product functions:

$$w_{s,t}(x, y) = f(x - s)f(y - t). \tag{22}$$

All commonly used schemes fit into the system defined by the constraints given in this section. The general force law and the spline fitting schemes appear as a subset of the schemes defined by the multipole expansion used for the coulombic force. In all cases, higher-order constraints may be satisfied by increasing the number of points to which charge from each particle is assigned.

If the computational cost of charge assignement were of little account, then a spline fitting scheme would be the best choice. However, to achieve an order n long-range force error under the spline fitting constraints requires charge assignment to $(n + 1)^2$ points rather than the $(2n + 1)$ points per particle required by the coulombic force law constraints (Eq. (12)). Since the physics of collisionless plasmas depends on the long-range interactions, the computationally cheaper schemes defined by (12) may represent practical alternatives, provided that the short-range force errors do not severely degrade collision and heating times.

3. Examples of Charge-Sharing Schemes

The lowest-order charge-sharing scheme is obtained by satisfying only the $n = 0$ constraint. This is achieved by assigning charge to the nearest grid point (NGP);

$$w_{0,0}(x, y) = \begin{cases} 1; & -\frac{1}{2} < x \leqslant \frac{1}{2}\,, \quad -\frac{1}{2} < y \leqslant \frac{1}{2}\,, \\ 0; & \text{otherwise.} \end{cases} \tag{23}$$

Extending charge assignment to the three nearest grid points to a particle,

enables the $n = 0$ and 1 constraints (Eq. (12)) to be satisfied. The resulting first-order scheme is

$$w_{0,0}(x, y) = \begin{cases} 1 - |x| - |y|; & -\frac{1}{2} < x \leqslant \frac{1}{2}, \quad -\frac{1}{2} < y \leqslant \frac{1}{2}, \\ 1 - |x|; & -\frac{1}{2} < y \leqslant \frac{1}{2}, \quad -1 < x \leqslant -\frac{1}{2}, \quad \frac{1}{2} < x \leqslant 1, \\ 1 - |y|; & -\frac{1}{2} < x \leqslant \frac{1}{2}, \quad -1 < y \leqslant -\frac{1}{2}, \quad \frac{1}{2} < y \leqslant 1, \\ 0; & \text{otherwise.} \end{cases} \tag{24}$$

Physically, the scheme (24) may be regarded as placing all the charge at the nearest grid point, together with dipoles parallel to the x and y axes of strength proportional to $|x|$ and $|y|$, respectively.

In a similar manner, we find the four-point scheme satisfying the $n = 0$ and $n = 1$ constraints (Eq. (12)):

$$w_{0,0}(x, y) = \begin{cases} \alpha(|x|, |y|); & -\frac{1}{2} < x \leqslant \frac{1}{2}, \quad -\frac{1}{2} < y \leqslant \frac{1}{2}, \\ 1 - |x| - \alpha(|x|, 1 - |y|); & \\ & -\frac{1}{2} < x \leqslant \frac{1}{2}, \quad -1 < y \leqslant -\frac{1}{2}, \quad \frac{1}{2} < y \leqslant 1, \\ 1 - |y| - \alpha(1 - |x|, |y|); & \\ & -\frac{1}{2} < y \leqslant \frac{1}{2}, \quad -1 < x \leqslant -\frac{1}{2}, \quad \frac{1}{2} < x \leqslant 1, \\ 1 - |x| - |y| + \alpha(1 - |x|, 1 - |y|); & \\ \quad -1 < x \leqslant \frac{1}{2}, \quad \frac{1}{2} < x \leqslant 1, \quad -1 < y \leqslant -\frac{1}{2}, \quad \frac{1}{2} < y \leqslant 1, & \\ 0; \quad \text{otherwise,} & \end{cases} \tag{25}$$

where α is some arbitrary function. One choice of α,

$$\alpha(|x|, |y|) = 1 - |x| - |y|, \tag{26}$$

reduces (25) to the three-point scheme, while another,

$$\alpha(|x|, |y|) = (1 - |x|)(1 - |y|), \tag{27}$$

reduces (25) to a bilinear function:

$$w_{0,0}(x, y) = \begin{cases} (1 - |x|)(1 - |y|); & |x| \leqslant 1, \quad |y| \leqslant 1, \\ 0; & \text{otherwise.} \end{cases} \tag{28}$$

The scheme given by (28) is the linear spline charge-weighting scheme, also known as area weighting and the CIC scheme [9, 10]; other choices of the function α may prove advantageous, although what particular form it should take has not yet been investigated.

Extending charge assignment to five mesh points allows the second-order constraints (12) to be satisfied. Alternatively, the first-order constraints may be satisfied, leaving two arbitrary functions to adjust the short-range force behavior.

In a like manner, schemes may be devised for charge sharing over six, seven or more mesh points, allowing progressively higher-order constraints to be accommodated. The problem with many of the possible schemes is that considerable effort is expended deciding where the odd points are to be placed, unless there is a regular invariant pattern of points, as in the four-point, symmetrical five-point, or nine-point schemes.

A variety of schemes satisfying the lower-order terms of (12) are possible when charge is assigned to the nine mesh points closest to each particle. For instance, constraints to third order may be satisfied, leaving two free parameters to adjust the short-range force behavior. Alternatively, a second-order scheme using biquadratic charge-weighting function may be chosen:

$$w_{0,0}(x, y) = f(x)f(y), \tag{29}$$

where

$$f(x) = \begin{cases} 1 - c - x^2; & -\frac{1}{2} < x \leqslant \frac{1}{2}, \\ \frac{1}{2}(x^2 - 3 \mid x \mid + 2 + c); & -\frac{3}{2} < x \leqslant -\frac{1}{2}, \quad \frac{1}{2} < x < \frac{3}{2}, \\ 0; & \text{otherwise.} \end{cases} \tag{30}$$

In particular if the constant c is set to $\frac{1}{4}$, then (29) and (30) correspond to a finite-sized particle with a shape factor given by the product of triangle functions (cf. the product of "top-hat" functions for the CIC scheme). This scheme, the Triangular Shaped Cloud (TSC) scheme, when combined with the adjustment of the kernel in the field equation gives the quadratic spline scheme [17]. In Part II we shall investigate a semiempirical approach to the adjustment of the kernel of the field equation for arbitrary charge-sharing schemes.

As a final example of charge-sharing scheme, we consider the nine-point gaussian-shaped cloud scheme, whose shape factor is

$$S(x, y) = (1/2\pi\sigma^2 \operatorname{erf}^2(1/(2\sigma)^{1/2})) \exp[-(x^2 + y^2)/2\sigma^2]. \tag{31}$$

Choosing different values of σ leads to different constraint equations being satisfied. For instance, $\sigma = .40$ satisfies the $n = 0$ and 1 constraints (12), while $\sigma = .54$ satisfies the $n = 0$ and $n = 2$ constraints (Eqs. (12) and (17)). A compromise choice of $\sigma = 0.455$ gives a weighting function quite close to TSC over most of the range. This cloud which will be referred to as the GSC is used in the empirical comparisons of Part II.

4. Shaping the Force Law at Short Range

The mesh of potential values $\{\phi_{s,t}\}$ and field values $\{\mathbf{E}_{s,t}\}$ are related to the mesh charge distribution by the convolution sums:

$$\phi_{s,t} = \frac{q}{\epsilon_0} \sum_{s',t'} G_{s-s',t-t'} \rho_{s',t'} , \tag{32}$$

$$\mathbf{E}_{s,t} = \frac{q}{\epsilon_0} \sum_{s',t'} \mathbf{d}_{s-s',t-t'} \rho_{s',t'} , \tag{33}$$

where the sums (s', t') are taken over all mesh points. Generally, the electric field influence (or Green's) function $\mathbf{d}_{s,t}$ is related to the potential influence function $G_{s,t}$, by some simple difference equation, although this is not a necessary condition.

Using (33), we may write the force $\mathbf{F}$ at (x_1 , y_1) due to a source charge at (x_0 , y_0):

$$\mathbf{F} = q^2 \sum_{s_1,t_1,s_2,t_2} w_{s_1,t_1}(x_0 , y_0)\, w_{s_2,t_2}(x_1 , y_1)\, \mathbf{d}_{s_2-s_1,t_2-t_1} . \tag{34}$$

In order to represent a central force of interaction, the mesh force given by (34) should be a function only of the distance separating the source and field points and be directed along the line joining them. However, owing to the introduction of the mesh, there is a nonzero force perpendicular to the line of centers and the magnitude of the force will depend on the location of the source and field points with respect to the mesh, as well as on their separation.

These nonphysical effects are most pronounced at short range and it is the purpose of this section to show how they may be reduced by modifying the influence function G, without altering the force law at long range.

To measure the quality of the representation we introduce a reference central force $\mathbf{R}$. A measure of how close $\mathbf{F}$ gets to $\mathbf{R}$ is given by their squared difference, integrated over all positions of the source and field points:

$$Q = \int_{-1/2}^{1/2}\int dx_0\, dy_0 \int_{-\infty}^{\infty}\int dx_1\, dy_1\, (\mathbf{F} - \mathbf{R})^2. \tag{35}$$

If the charge-sharing scheme is derived according to the constraints given in Section 2, then the integrand of (35) decays like $r^{-2(n+1)}$, where r is the particle separation and n is the order of the charge-sharing scheme. Consequently, (35) may be truncated with little loss of accuracy:

$$Q^* = \int_{-1/2}^{1/2}\int dx_0\, dy_0 \int_{-m}^{m}\int dx_1\, dy_1\, (\mathbf{F} - \mathbf{R})^2. \tag{36}$$

From (33) and (34) we see that Q^* is a quadratic function of the influence function $\mathbf{d}_{s,t}$, and hence Q^* is also a quadratic function of the potential influence function $G_{s,t}$ provided that the field is obtained from the potential by differencing. Consequently for a particular charge-sharing, potential-differencing, and reference-force combination, there is a unique optimal set of coefficients $\{G^*_{s,t}\}$ which minimize Q^*.

The adjustment of the influence function is interpreted as a shaping of the charged rods. The force between charges is coulombic, with a cutoff at short range being due to the finite diameter of the charges, i.e., the shape of the charges is measured by the reference force law, rather than by the charge-sharing scheme. The optimal set of values $\{G^*_{s,t}\}$ are thus those which produce a mesh expanded force that most accurately imitates the real force between two finite-sized charged rods.

The advantage of this charge-shaping method over other smoothing techniques is that it leads to no increase in the cycle time of a particle-mesh calculation provided that finite Fourier transforms (FFT) are employed to solve the field equation. The FFT of (32) gives the harmonic equations:

$$\hat{\phi}_{k,l} = (-H^2/\epsilon_0)\, \hat{G}_{k,l}\hat{\rho}_{k,l}\,, \tag{37}$$

where $\hat{G}_{k,l}$ is the transform of $G_{s,t}$.

$$G_{s,t} = \frac{1}{N^2} \sum_{s,t=-N/2}^{N/2-1} \hat{G}_{k,l} \exp\left[\frac{i2\pi}{N}(ks + lt)\right], \tag{38}$$

and $\hat{\phi}_{k,l}$ and $\hat{\rho}_{k,l}$ are the potential and charge harmonics, respectively, for an N-by-N periodic square mesh with mesh spacing H. If $\{G_{s,t}\}$ and $\{G^*_{s,t}\}$ differ only for $|s| < m$, $|t| < m$, and we make use of the symmetry conditions $G_{-s,t} = G_{s,-t} = G_{s,t}$, the summation can be put in the convenient real form:

$$\hat{G}^*_{k,l} = \hat{G}_{k,l} + \sum_{s,t=0}^{m} c_{s,t} \cos\frac{2\pi ks}{N} \cos\frac{2\pi lt}{N}\,, \tag{39}$$

where the short-range potential correction coefficients, $c_{s,t}$, are defined by

$$c_{s,t} = (2 - \delta_{s,0})(2 - \delta_{t,0})(G^*_{s,t} - G_{s,t}).$$

The empirical determination of the coefficients $c_{s,t}$ is given in Part II, and since there is nothing to distinguish the x and y directions one must have $c_{s,t} = c_{t,s}$. In any practical computation $\{\hat{G}^*_{k,l}\}$ is precalculated, so the modification of the potential calculation is introduced via (39) with, as noted above, no effect on the cycle time.

To illustrate the nature of the changes effected by varying the potential correction coefficients, we shall consider an algorithm using a nine-point scheme where only the $c_{1,0} = c_{0,1}$ coefficients are nonzero. Potential values due to a charge at mesh point (s, t) are modified only at neighboring locations $(s + 1, t)$, $(s - 1, t)$, $(s, t + 1)$ and $(s, t - 1)$. The cumulative effect of these altered potentials is followed in Fig. 1.

Figure 1a shows the assignment of the charge of a rod lying in cell (0, 0) to the nine nearest neighboring mesh points (boldfaced dots). Mesh points at which

potentials are modified are shown boldface in Fig. 1b, followed in Fig. 1c by mesh points at which field values are affected (here, a two-point centered difference for the electric field is assumed for the purpose of illustration). Finally, in Fig. 1d is shown the area over which the interparticle force is influenced; any charge

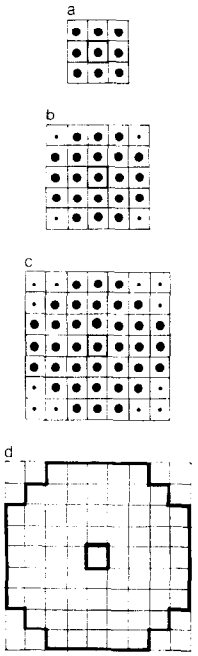

FIG. 1. The localized nature of the force shaping resulting from charging coefficient c_{10}; (a) charge assignments, (b) potential, (c) electric field, and (d) force. See text for further details.

lying outside the box symmetrically placed about the cell (0, 0) feels a force due to the charge in cell (0, 0) which is independent of $c_{1,0}$. Similar representations may be sketched for cases where other potential coefficients, charge-sharing schemes and difference equations for the field are involved.

The influence function for the example shown in Fig. 1 is

$$\hat{G}^*_{k,l} = \hat{G}_{k,l} + c_{1,0}[\cos(2\pi k/N) + \cos(2\pi l/N)]. \tag{40}$$

Assuming that $\hat{G}_{k,l}$ is derived from a "Poisson" equation,

$$D^2\phi_{s,t} = -\rho_{s,t}/\epsilon_0\,, \tag{41}$$

where D^2 is some finite-difference approximation to the laplacian operator,

then the solution to (32) using the modified influence function (40) in (37) is equivalent to charge reshaping before solving for the potential using (42):

$$\rho^*_{s,t} = [1 + \tfrac{1}{2} \cdot c_{1,0} D^2 S_{1,0}]\, \rho_{s,t}\,; \tag{42}$$

or to potential smoothing after solving (41):

$$\phi^*_{s,t} = [1 + \tfrac{1}{2} \cdot c_{1,0} S_{1,0} D^2]\, \phi_{s,t}\,. \tag{43}$$

$S_{1,0}$ is the symmetric sum operator:

$$S_{1,0}\psi_{s,t} = \psi_{s-1,t} + \psi_{s+1,t} + \psi_{s,t-1} + \psi_{s,t+1}\,. \tag{44}$$

Part II. Empirical Results

We now present a series of empirical results which show numerically the extent to which the law of force between two interacting model particles can be shaped by different choices of the cloud, the Poisson solver and the potential-correction coefficients. We find that the quality of the long-range force is primarily determined by the choice of the Poisson solver and that the quality of the short-range force is primarily determined by the cloud shape and the potential-correction coefficients. In terms of Eq. (39), for a given cloud shape, the long-range force is determined by the choice of $\hat{G}_{k,l}$ and the short-range force by the choice of $c_{s,t}$. All forces are quoted as absolute measures and expressed as fractions or percentages of the coulombic force at one mesh distance ($=q^2/2\pi\epsilon_0 H$). The absolute measure is adopted because the stochastic heating rate, which measures the combined effect of all computational errors, is proportional to the mean square value of the absolute error in the electric field [18].

5. The Long-Range Force

Four different Poisson solvers have been compared. These can be defined by giving the Fourier transform multiplying factor $\hat{G}_{k,l}$.

(a) *Truncated* $-1/k^2$ *Fourier Series*

The Fourier transformation of Poisson's equation with doubly periodic boundary conditions gives an infinite Fourier series. The truncation of the coefficients to the range of the finite transform leads to the following Poisson solver.

$$\begin{aligned} \hat{G}_{k,l} &= N^2/4\pi^2(k^2 + l^2), \qquad 0 \leqslant k, l \leqslant N/2, \quad k = l \neq 0, \\ &= 0, \qquad k = l = 0 \quad \text{and} \quad (k^2 + l^2)^{1/2} > N/2. \end{aligned} \tag{45}$$

This type of Poisson solver, called by Boris the Poor man's Poisson solver [19], is often favored because it is derived directly from the differential equation without finite-difference approximations. This advantage is illusory because no account is taken of harmonic aliasing in (45) which arises due to the finite sampling of the solution by the mesh, and the behavior of the approximation is poor. The finite-difference approximations which follow include the effect of aliasing in a natural way. Different forms of truncation may be used in Eq. (45). We have chosen a truncation that is a function only of modulus of the wave number in order to counteract the squareness of the mesh as much as possible.

(b) *Nine-Point Finite Difference*

The nine-point finite-difference approximation to Poisson's equation [20] is represented by the stencil equation:

$$\begin{bmatrix} 1/6 & 2/3 & 1/6 \\ 2/3 & -10/3 & 2/3 \\ 1/6 & 2/3 & 1/6 \end{bmatrix} \phi_{s,t} = -\frac{H^2}{\epsilon_0} \begin{bmatrix} 0 & 1/12 & 0 \\ 1/12 & 2/3 & 1/12 \\ 0 & 1/12 & 0 \end{bmatrix} \rho_{s,t}, \tag{46}$$

where the matrix of numbers gives the coefficients which multiply the mesh values in the corresponding positions.

Applying the finite double Fourier transform to (46) gives

$$\begin{aligned} &\hat{G}_{kl} = (A + 4)/(4B + 8A - 20), \qquad k, l = 0, 1, \ldots, N/2, \quad k = l \neq 0, \\ &\hat{G}_{00} = 0, \end{aligned} \tag{47}$$

where

$$\begin{aligned} A &= \cos(2\pi k/N) + \cos(2\pi l/N), \\ B &= \cos(2\pi k/N)\cos(2\pi l/N). \end{aligned} \tag{48}$$

(c) *Five-Point Finite Difference*

The five-point finite-difference approximation to Poisson's equation is defined by the stencil:

$$\begin{bmatrix} 0 & 1 & 0 \\ 1 & -4 & 1 \\ 0 & 1 & 0 \end{bmatrix} \phi_{s,t} = -\frac{H^2}{\epsilon_0} \rho_{s,t}, \tag{49}$$

or the multiplying factor:

$$\begin{aligned} &\hat{G}_{k,l} = 1/(2A - 4), \qquad k, l = 0, 1, \ldots, N/2, \quad k = l \neq 0, \\ &\hat{G}_{0,0} = 0. \end{aligned} \tag{50}$$

(d) *Diagonal Five-Point Finite Difference*

The five-point finite difference may be rotated through 45° to obtain the diagonal five-point stencil:

$$\begin{bmatrix} 1/2 & 0 & 1/2 \\ 0 & -2 & 0 \\ 1/2 & 0 & 1/2 \end{bmatrix} \phi_{s,t} = -\frac{H^2}{\epsilon_0} \begin{bmatrix} 0 & 1/8 & 0 \\ 1/8 & 1/2 & 1/8 \\ 0 & 1/8 & 0 \end{bmatrix} \rho_{s,t}, \tag{51}$$

and

$$\hat{G}_{k,l} = (A + 2)/(8(B - 1)).$$

We consider the long-range force to be that for which $r > 4H$, because the potential-correction coefficients will be used to shape the force when $r < 4H$. The quality of the long-range force was assessed by observing the force in the model between a single positive and a single negative charged particle, and comparing this with the exact elliptic-function expression (52) for the force, $E(z)$, between two line charges, periodically repeated:

$$E(z) = E_x - iE_y = q^2\{Z(z_1) + (\pi i y_1/2KK')\}(2K/L)/2\pi\epsilon_0, \tag{52}$$

where $z_1 = (L/2 - z)(2iK/L)$, and $z = (x + iy)$ is the complex separation between

TABLE I

Error in the Force between Two Interacting Rods of Charge per Unit Length, q, for Different Clouds and Poisson solvers in Units of $10^{-5}(q^2/2H\epsilon_0 H)$

Cloud	Poisson	$r = 4H$	$8H$	$16H$	$32H$
CIC	$-1/k^2$	1500	280	54	29
	nine-point	610[a]	71[a]	10[a]	2
	x–y five-point	960	100	12	1[a]
	diag five-point	1300	160	23	5
TSC	$-1/k^2$	730	120	22	11
	nine-point	650[a]	71[a]	10[a]	2
	x–y five-point	820	98	13	1[a]
	diag five-point	1200	180	24	5
GSC	$-1/k^2$	740	120	22	10
	nine-point	650[a]	71[a]	9[a]	2
	x–y five-point	820	99	12	1[a]
	diag five-point	1189	183	25	5

[a] Designates the best Poisson solver for each cloud.

the particles which have charge per unit length q. K and K' are the complete elliptic integrals of the first kind and $L = NH$ the periodic-repeat distance. $Z(z)$ is the Jacobean Zeta function [21].

The positive particle was placed on a mesh point and the negative particle a variable distance r from it, such that the line between the particles made an angle, θ, with the x-axis. A square doubly periodic 64×64 mesh was used with defining vectors parallel to the x- and y-axis. The force was resolved into components F_r parallel to, and F_θ, perpendicular to the line joining the particles.

Table I shows, for three cloud shapes and four Poisson solvers, the maximum deviation of F_r and F_θ from the exact value of Eq. (52). The comparison was made for $\theta = 0$, 11.25, 22.5, 33.75, and 45° at $r = 4$, 8, 16, and $32H$. It can be seen that, with the exception of $r = 32H$, the nine-point Poisson solver is the most accurate for all cloud shapes. It is not possible to distinguish between TSC and GSC interpolation, both of which have significantly better long-range behavior than CIC. We note also that the truncated $-1/k^2$ Poisson solver is considerably worse than both the nine- and five-point finite-difference Poisson solvers, particularly at large distances.

6. The Short-Range Force

The short-range force for $r < 6H$ is shown in Fig. 2, the solid lines representing the law of force between two particles as measured parallel to the mesh axis ($\theta = 0$), and the dotted lines represent the law of force as measured diagonally through the

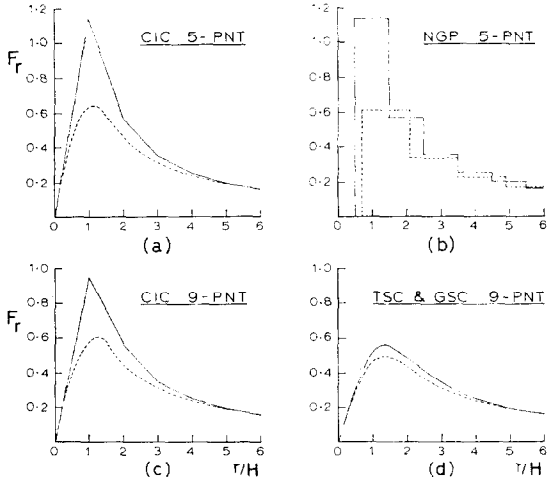

FIG. 2. Short-range force law. The angular anisotropy of the force law for different clouds and potential solvers. Solid curve $F_r(r, 0°)$, dotted curve $F_r(r, 45°)$. Force in units of $q^2/2\pi\epsilon_0 H$.

mesh ($\theta = 45$). Measurements have been made at three intermediate angles and are found to lie between the curves shown. In all cases the first particle lies on a mesh point. Measurements have also been made for eight different positions of the first particle in a cell. Different force laws are obtained depending on the position of the first particle, however the magnitude of the anisotropy of the force is similar to the curves shown which may be considered to be typical for the cloud and Poisson solver quoted.

Figure 2(a) and 2(b) show the short-range force law for the two simplest schemes, namely the CIC and NGP with the five-point Poisson solver. In both cases the force at one mesh distance varies by 50 % between $\theta = 0$ and 45°. It is interesting that, although the CIC interpolation gives a smoother force law than NGP, it does not reduce the large angular anisotropy of the force. Adoption of the nine-point Poisson solver reduces the angular anisotropy to 35 %. Figure 2(c) shows the force law for CIC. We do not show the curve for NGP since this is almost identical to Fig. 2(b) except that the first step for $\theta = 0$ is reduced in height from 1.14 to 0.95.

Figure 2(d) shows the force law for both the TSC and GSC clouds and the nine-point Poisson solver. The two cases differ by less than 0.4 %, and it can be seen that the adoption of nine-point charge-sharing and Poisson approximation has reduced the angular anisotropy to ~6 % (6.6 % for TSC and 6.2 % for GSC).

7. The Potential-Correction Coefficients

The effect of introducing the short-range potential-correction coefficients is shown in Fig. 3. The two cases shown both use the GSC and nine-point Poisson solver. Case (a) uses two independent coefficients ($c_{00} = 0.226$ and $c_{01} = c_{10} =$

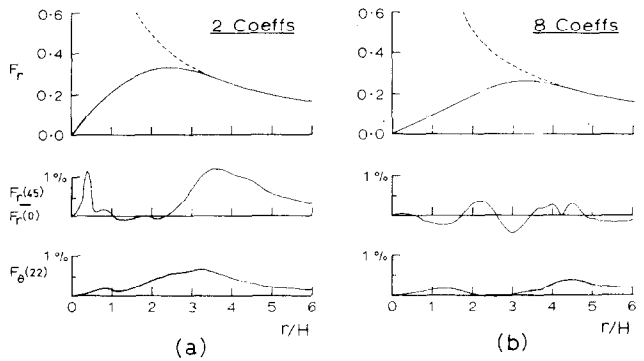

FIG. 3. Potential Correction. The improvement in the isotropy of the force resulting from the use of two and eight potential-correction coefficients. Solid curve is the force in the model. Dotted curve is the exact force between line charges. Force in units of $q^2/2\pi\epsilon_0 H$.

0.140) and the anisotropy of the force, as measured by $F_r(45°) - F_r(0°)$, is reduced from about 6% to about 1%. The F_θ is similarly reduced to less than 1%. The resulting force law starts from zero at $r = 0$, rises to a maximum value of $F_r = F_{\max}$ at $r = W$, and then joins smoothly into the exact elliptic-function expression (dotted line). Such a force law is characteristic of the interaction between two clouds of charge of width W and approximately uniform density. In Case (a) we have produced a good approximation to the interaction between clouds of width $W = 2.4H$ and $F_{\max} = 0.33$. In order to obtain a further significant reduction in the anisotropy, it is necessary to introduce eight independent coefficients:

$$c_{0,0} = 0.2804, \quad c_{0,1} = c_{1,0} = 0.2698, \quad c_{1,1} = 0.1775,$$
$$c_{0,2} = c_{2,0} = 0.0213, \quad c_{1,2} = c_{2,1} = 0.0878, \quad c_{2,2} = -0.0443,$$
$$c_{0,3} = c_{3,0} = 0.0067, \quad c_{1,3} = c_{3,1} = -0.0351.$$

With these coefficients the error in the force is reduced to less than 0.5% as shown in Fig. 3(b). The resulting particle width is $W = 3.3H$ and $F_{\max} = 0.257$. The model with these coefficients has been previously described as the Quiet Particle Mesh (QPM) model and has a stochastic heating rate less than one hundredth of the CIC five-point model [22].

The above correction coefficients were obtained by the following least-squares procedure. $F_r(r, \theta)$ and $F_\theta(r, \theta)$ are measured for $r/H = 0.5, 1.0, \ldots, 6.0$ and $\theta = 0$, 11.25, 22.5, 33.75 and 45°. The following constraints are applied:

along $\theta = 11.25, 22.5, 33.75°$,

$$F_r(r, \theta) - F_r(r, 0) = 0,$$

and (53)

$$F_\theta(r, \theta) = 0,$$

along $\theta = 45°$

$$F_r(r, 45) - F(r, 0) = 0, \qquad 0.5 < r/H < 3.5,$$
$$F_r(r, 45) - E_r(r) = 0, \qquad 3.5 \leqslant r/H \leqslant 6.0.$$

The resulting 88 equations for two or eight unknowns, respectively, were solved by least squares using the IBM SSP Library routines APFS and APLL.

The spatial averaging over different source points ($\iint dx_0\, dy_0$ in Eq. (35)) was achieved by determining the coefficients for nine different positions for the source particle and subsequently taking the area average of the coefficients. The positions used for the source particle were the cell center, the four corners of a cell, and the center of the four sides of a cell.

In the PPPM model [22] an arbitrary force is added to the above mesh force when the particle separation $r < a = 4H$. For this reason it is only important that the mesh force be independent of θ for $r < a$, the form of the dependence on r being unimportant. For $r > a$, it is important that the force be a good approximation to the coulombic force. For Case (a) we find that deviation from the exact force is less than 0.9 % and for Case (b) less than 0.43 %. For $r > 6H$ the potential coefficients no longer influence the force of interaction and the values in Table I are appropriate.

8. Points-In-A-Plane Force Law

The above procedure for shaping the r^{-1} force law between infinitely long rods of charge has been applied equally successfully to the r^{-2} force law of point charges confined to move in a plane. Such a force law is required in the study of surface films of electrons on liquid helium [23] and the interaction of ions in planar sheets.

The Fourier transform potential solver (37) was used with $\hat{G}$ chosen to give the exact potential at mesh points for a distribution of charge given only on the mesh points. Correct account was taken of contributions from all wave-number aliases. The potential-correction coefficients for use with the GSC were:

$$c_{0,0} = 0.4284, \quad c_{0,1} = c_{1,0} = -1.0985, \quad c_{1,1} = -0.8949,$$
$$c_{0,2} = c_{2,0} = -0.1585, \quad c_{1,2} = c_{2,1} = -0.2491, \quad c_{2,2} = -0.0192,$$
$$c_{0,3} = c_{3,0} = -0.0321, \quad c_{1,3} = c_{3,1} = 0.0982.$$

With these coefficients the force anisotropy is less than 0.15 % of the force at one mesh distance ($= q^2/4\pi\epsilon_0 H^2$).

Conclusions

A unified hierarchical theory has been presented for the shaping of the force law by the selection of charge-sharing and force-interpolation schemes. The first two terms in the hierarchy are the familiar NGP and CIC schemes, followed by the triangular shaped cloud (TSC). Empirical results are given showing that the TSC and the closely similar gaussian-shaped cloud (GSC) reduce the angular anisotropy of the force law from about 50 % for NGP and CIC to about 6 %. A further reduction of the anisotropy is obtained by introducing potential-correction coefficients which modify the multiplying factor used during the solution of Poisson's equation. Results are given using two and eight coefficients which reduce the anisotropy further to 1 and 0.5 %, respectively.

ACKNOWLEDGMENTS

The authors wish to acknowledge the financial support of UKAEA via an extramural contract, and the computer facilities provided by SRC on the RHEL 370/195 on which the empirical results were obtained. The willing assistance, when required, of the staff at the Atlas and RHEL laboratories is appreciated.

REFERENCES

1. R. W. HOCKNEY, *Meth. Computational Phys.* **9** (1970), 135.
2. R. W. HOCKNEY, *Phys. Fluids*, **9** (1966), 1826.
3. R. W. HOCKNEY, *J. Computational Phys.* **8** (1971), 19.
4. A. B. LANGDON, in "Proceedings of 4th Annual Conference on Numerical Simulation of Plasmas," N.R.L., Washington DC, 1970.
5. A. B. LANGDON AND C. K. BIRDSALL, *Phys. Fluids*, **13** (1970), 2115.
6. A. B. LANGDON, *J. Computational Phys.* **6** (1970), 247.
7. H. OKUDA, in "Proceedings of 4th Annual Conference on Numerical Simulation of Plasmas," N.R.L., Washington DC, 1970.
8. R. L. MORSE AND C. W. NIELSON, in "Proceedings of APS Top. Conference on Numerical Simulation of Plasmas," Los Alamos Report LA 3990 (1968).
9. R. L. MORSE, *Meth. Computational Phys.* **9** (1970), 213.
10. C. K. BIRDSALL, A. B. LANGDON AND H. OKUDA, *Meth. Computational Phys.* **9** (1970), 241.
11. J. H. ORENS, J. P. BORIS, AND I. HABER, in "Proceedings of 4th Annual Conference on Numerical Simulation of Plasmas," N.R.L., Washington, DC, 1970.
12. W. L. KRUER, J. M. DAWSON, AND B. ROSEN, *J. Computational Phys.* **13** (1973), 114.
13. B. ROSEN, W. L. KRUER, AND J. M. DAWSON, in "Proceedings of 4th Annual Conference of Numerical Simulation of Plasmas, N.R.L., Washington, DC, 1970.
14. H. R. LEWIS, *J. Computational Phys.* **6** (1970), 136.
15. H. R. LEWIS, *Meth. Computational Phys.* **9** (1970), 307.
16. H. R. LEWIS, A. SYKES, AND J. A. WESSON, *J. Computational Phys.* **10** (1972), 85.
17. O. BUNEMAN, *J. Computational Phys.* **11** (1973), 250.
18. R. W. HOCKNEY, *Phys. Fluids* **11** (1968), 1381.
19. J. P. BORIS AND K. V. ROBERTS, *J. Computational Phys.* **4** (1969), 552.
20. L. V. KANTOROVICH AND V. J. KRYLOV, "Approximate Methods in Higher Analysis" (translated by C. D. Benster), P. NoordHoff Ltd., Groningen, Netherlands, 1958, Pg. 186.
21. M. ABROMOWITZ AND I. A. STEGUN, "Handbook of Mathematical Functions," U.S. Department of Commerce, National Bureau of Standards Applied Mathematics Series 55, U.S. Government Printing Office Washington DC, 1964, Pg. 578.
22. R. W. ROCKNEY, S. P. GOEL, AND J. W. EASTWOOD, *J. Computational Phys.* **14** (1974), 148.
23. M. W. COLE AND M. H. COHEN, *Phys. Rev. Lett.* **23** (1969), 1238.